Applied Catalysis B: Environmental 148–149 (2014) 490–498

Contents lists available at ScienceDirect

Applied Catalysis B: Environmental

journal homepage: www.elsevier.com/locate/apcatb

$LaMnO_3$ perovskite oxides prepared by different methods for catalytic oxidation of toluene

Chuanhui Zhang[a,b], Yanglong Guo[a,*], Yun Guo[a], Guanzhong Lu[a], Antoinette Boreave[b], Laurence Retailleau[b], Alexandre Baylet[b], Anne Giroir-Fendler[b,**]

[a] Key Laboratory for Advanced Materials and Research Institute of Industrial Catalysis, East China University of Science and Technology, Shanghai 200237, China

[b] Université Lyon 1, CNRS, UMR 5256, IRCELYON, Institut de recherches sur la catalyse et l'environnement de Lyon, 2 Avenue Albert Einstein, 69626 Villeurbanne Cedex, France

ARTICLE INFO

Article history:
Received 31 July 2013
Received in revised form
15 November 2013
Accepted 19 November 2013
Available online 27 November 2013

Keywords:
Perovskite
Sol–gel synthesis
Toluene oxidation
Low-temperature reducibility
Surface adsorbed oxygen

ABSTRACT

Perovskite-type oxides of $LaMnO_3$ (LMO) were synthesized by citrate sol–gel (SG), glycine combustion (GC) and co-precipitation (CP) methods, respectively. The physicochemical properties of these $LaMnO_3$ materials were characterized by XRD, N_2 sorption, H_2-TPR and O_2-TPD. Their catalytic performances were evaluated for the oxidation of toluene. It was shown that well-formed perovskite structures were obtained over samples LMO-SG and LMO-GC. Traces of La_2O_3 phase were detected over sample LMO-CP. The ranking in terms of specific surface area, low-temperature reducibility and concentration of surface adsorbed oxygen species from the highest to the lowest value was LMO-SG > LMO-CP > LMO-GC, which was in good agreement with the catalytic activity order. Sample LMO-SG exhibited the optimum catalytic activity and durability without any deactivation observed during the steady state of 60 h. Its superior catalytic performance could be greatly attributed to its higher specific surface area, better low-temperature reducibility and more available surface adsorbed oxygen species. The apparent activation energies of samples LMO-SG, LMO-GC and LMO-CP were 71, 84 and 76 kJ mol^{-1}, respectively. The lowest apparent activation energy of sample LMO-SG was in good agreement with its better catalytic behavior for toluene oxidation.

1. Introduction

Volatile organic compounds (VOCs) are greatly emitted from industrial process, automobile exhaust emissions and human daily activities. VOCs are not only regarded as one of the most contributors to air pollution, for instance, causing the formation of photochemical smog [1,2], but also as the main hazardous substances with great damage effect on public health because of their toxic, mutagenic and carcinogenic properties. Therefore, many countries and organizations such as USA, European Union (EU) and Japan introduced stringent legislations and regulations to control release of VOCs emissions [3–5].

In order to efficiently remove VOCs, various technologies are developed, mainly including adsorption, bio-degradation, membrane separation, thermal incineration, catalytic oxidation and photocatalytic oxidation. Among these technologies, catalytic oxidation is considered as the most promising alternative process for elimination of VOCs emissions due to its low operation temperature, low level of energy consumption and high purification efficiency. During the past periods, supported precious metals [6,7], transition metal oxides [8–10] and perovskite oxides [11–13] have been widely used as catalysts for catalytic oxidation of numerous VOCs. Although supported precious metal catalysts are highly active and efficient for VOCs combustion, their high costs are uneconomical and unpractical for large-scale industrial applications. With the increasing demand for cheaper and more environmentally friendly catalytic materials, avoiding the use of precious metals and searching other inexpensive and active catalysts become a hot subject in the present studies.

As one of the substitutes for precious metal catalysts, perovskite-type metal oxides, more specifically $LaMnO_3$-based perovskites, have attracted much attention due to their adequate catalytic activity and good thermal stability for catalytic oxidation of various hydrocarbons. For example, Spinicci et al. [14] investigated the catalytic combustion of acetone, isopropanol and benzene over $LaMnO_3$ perovskites, finding that presence of surface oxygen species, easily available and sufficiently mobile, was the fundamental requirement for the high catalytic activity of $LaMnO_3$.

* Corresponding author. Tel.: +86 21 64 25 29 23; fax: +86 21 64 25 29 23.
** Corresponding author. Tel.: +33 4 72 43 15 86; fax: +33 4 72 43 16 95.
E-mail addresses: ylguo@ecust.edu.cn (Y. Guo), anne.giroir-fendler@ircelyon.univ-lyon1.fr (A. Giroir-Fendler).

0926-3373/$ – see front matter © 2013 Elsevier B.V. All rights reserved.
http://dx.doi.org/10.1016/j.apcatb.2013.11.030

Álvarez-Galván et al. [15] studied combustion of methyl ketone over La-transition metal (Cr, Co, Ni, Mn) perovskites, and $LaMnO_3$ catalyst exhibited the optimum catalytic performance with a complete conversion of methyl ketone achieved at 297 °C. However, in order to assure the formation of perovskite structure, calcination of precursor material at high temperature (normally above 600 °C) is necessary, and thus leads to the relatively lower specific surface area and low-temperature reducibility in comparison with those of some other transition metal oxides. Therefore, in order to obtain perovskites with high specific surface area and outstanding redox activity, selection and optimization of the synthesis method is the key parameter.

In this work, $LaMnO_3$ perovskite oxides were synthesized by three different methods, namely citrate sol–gel (SG), glycine combustion (GC) and co-precipitation (CP), and their catalytic performances were evaluated for the catalytic oxidation of toluene as a model reaction. Series of characterization techniques including XRD, N_2 sorption, H_2-TPR and O_2-TPD were performed to investigate the correlation between the physicochemical properties and the catalytic performances over these $LaMnO_3$ perovskite oxides. In addition, the effect of Weight Hourly Space Velocity (WHSV) on the catalytic performance and the apparent activation energies of $LaMnO_3$ perovskite oxides for toluene oxidation were also studied.

2. Experimental

2.1. Catalyst preparation

Metal nitrates ($La(NO_3)_3{\cdot}6H_2O$ and $Mn(NO_3)_2{\cdot}4H_2O$) of analytical grade were used as precursors to prepare $LaMnO_3$ perovskite-type oxides. First, equimolar amounts of the nitrates were weighed and mixed in a beaker, and then an amount of distilled water was added to make an aqueous solution containing the nitrates mixture, which was named as solution A.

2.1.1. Citrate sol–gel method (SG)

An amount of citric acid (CA) with the molar ratio of CA to total metallic ions (sum of La^{3+} and Mn^{2+}) set at 1.2 was added to the previous solution A at room temperature (pH = 1). The formed citrates solution was heated at 80 °C for 2 h to evaporate excess amount of H_2O under magnetic stirring, then dried at 120 °C overnight. After the pretreatment in a muffle furnace at 200 °C (the heating rate of 2 °C min^{-1}) for 1 h, the resulting materials was finally calcined at 750 °C (the heating rate of 5 °C min^{-1}) for 2 h in a quartz tubular reactor under air atmosphere.

2.1.2. Glycine combustion method (GC)

An amount of glycine with the molar ratio of glycine to total metallic ions set at 2.0 was added to solution A at room temperature (pH = 6). The formed solution was heated at 80 °C for 2 h to allow it change into viscous slurry under magnetic stirring, and then dried at 120 °C overnight. After the pretreatment in a muffle furnace at 250 °C (the heating rate of 2 °C min^{-1}) for 1 h, the resulting materials was finally calcined at 750 °C (the heating rate of 5 °C min^{-1}) for 2 h in a quartz tubular reactor under air atmosphere.

2.1.3. Co-precipitation method (CP)

An aqueous solution with a molar ratio of $[NaOH]/[Na_2CO_3]$ of 2.0 as the precipitator was added dropwise to solution A under magnetic stirring until the pH value reached 10. After aging for 4 h at room temperature, the resulting suspension was filtered and thoroughly washed with distilled water. The same thermal treatment as the SG and GC methods was used to obtain perovskite oxides.

In order to facilitate the description, $LaMnO_3$ oxides prepared by the above methods were denoted as LMO-SG, LMO-GC and LMO-CP, respectively.

2.2. Catalyst characterization

Powder X-ray diffraction (XRD) patterns were recorded on a Bruker D5005 diffractometer equipped with a Cu $K\alpha$ radiation (λ = 1.5418 Å) and a graphite monochromator on the diffracted beam, and the XRD data was generally collected in the 2θ range of 10–80° with a step size of 0.05°. Nitrogen sorption at 77 K was performed on a Micromeritics Tristar 3000 surface area and porosity analyzer. Before the measurement, the samples were degassed at 300 °C for 3 h. The specific surface area (SSA) of each sample was obtained by Brunauer–Emmett–Teller (BET) method [16], and the pore volume and pore size distribution was calculated by Barrett–Joyner–Halenda (BJH) method [17]. Temperature programmed reduction of hydrogen (H_2-TPR) measurements were conducted on a self-designed setup equipped with a U-shaped quartz reactor and an INFICON IPC400 quadrupole mass spectrometer (MS). Prior to run, the sample (50 mg) was pretreated in a pure oxygen stream at 500 °C for 30 min to achieve a complete oxidation. After cooling down to room temperature, 30 mL min^{-1} of 5 vol% H_2/He mixture gas was introduced until stabilization of MS baseline. Then the reactor was heated at a ramp of 15 °C min^{-1} from room temperature to 930 °C. Simultaneously, the signal of consumed H_2 at m/e = 2 was recorded by MS detector. Temperature programmed desorption of oxygen (O_2-TPD) experiments were carried out on the same setup as H_2-TPR. Prior to each test, gaseous oxygen was previously adsorbed by a pretreatment of the sample (50 mg) at 550 °C for 60 min under pure oxygen atmosphere. After cooled down to room temperature, the reactor was purged by 30 mL min^{-1} of pure He until stabilization of MS baseline. Then the reactor was heated at a ramp of 15 °C min^{-1} from room temperature to 930 °C. Simultaneously, the signal of desorbed oxygen at m/e = 32 was recorded by MS detector.

2.3. Measurement of catalytic activity

Measurement of catalytic activity was performed in a conventional U-shaped tubular reactor placed in an electric furnace at atmospheric pressure. 240 mg of the catalyst, mixed with silicon carbide (SiC) to avoid the effect of hot spots, was deposited on a quartz wool plug, and the reaction temperature was continuously monitored by a thermocouple tied on the reactor and positioned at the middle of the catalyst bed. For the evaluation of catalytic activity, a mixture of O_2, toluene and He (20% O_2, 1000 ppm toluene vapor and He balance) with the total flow rate of 60 mL min^{-1}, corresponding to WHSV of 15,000 mL g^{-1} h^{-1}, was fed over the catalyst. The concentration of toluene was adjusted by a Calibrage PUL010 apparatus, which was constituted of a saturator and two He streams controlled by the mass flowmeters (BROOKS). One He stream was introduced into the saturator to maintain a constant flow rate of toluene vapor and the other one as gas balance. The reactor was heated from room temperature to 100 °C at the rate of 5 °C min^{-1}, maintained for 1 h at this temperature to avoid overestimation (caused by adsorption) of toluene conversion and then heated to 400 °C at the same heating rate and kept for 1 h at this temperature. Then, the reactor was cooled down to 100 °C naturally. The toluene and possible organic products were analyzed by an Agilent 6850 network gas chromatograph with a flame ionization detector (FID). CO_2 and CO were analyzed by a PerkinElmer Clarus 500 gas chromatograph equipped with a thermal conductivity detector (TCD). It was found that there was no other organic hydrocarbons in the products. Variation of WHSV was fulfilled by changing the catalyst mass at a fixed flow rate. Additionally, toluene

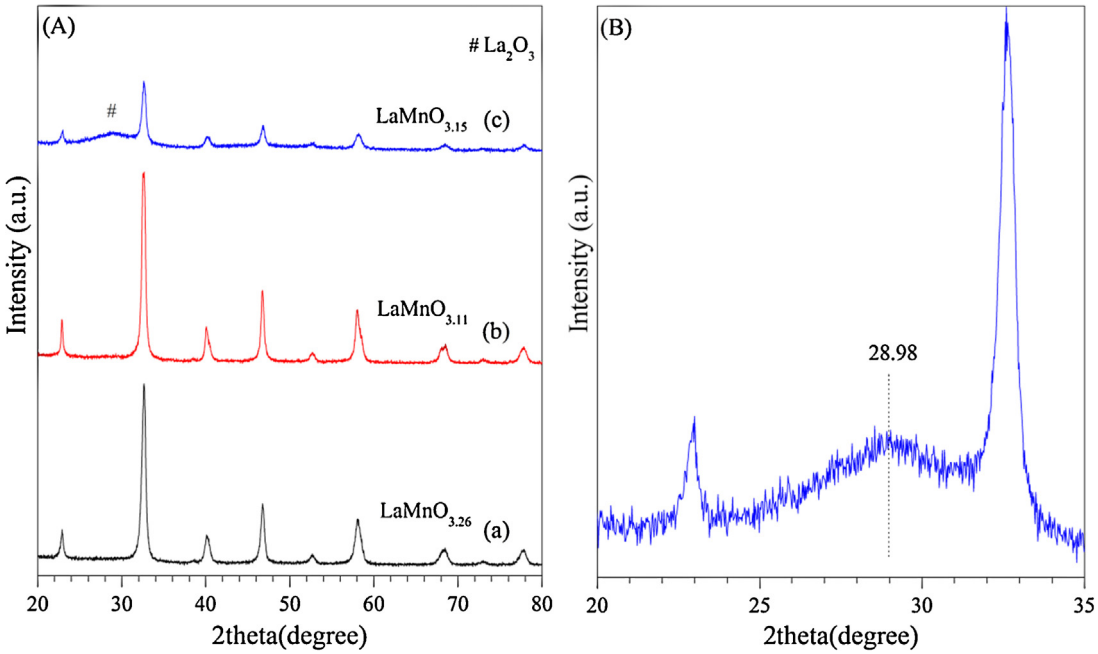

Fig. 1. (A) XRD patterns of samples (a) LMO-SG, (b) LMO-GC and (c) LMO-CP and (B) the partial XRD pattern of sample LMO-CP in the 2θ range of 20– 35°.

conversion and CO_2 yield over the catalysts were very similar, which indicated that CO_2 was the only carbon-containing product. The toluene conversion ($X\%$) and reaction rate r (mol g^{-1} s^{-1}) was calculated using the following equations:

$$X\% = \frac{[C_7H_8]_{in} - [C_7H_8]_{out}}{[C_7H_8]_{in}} \times 100$$

$$r = [C_7H_8]_{in} \times X\%/m_{cat} = \mathrm{WHSV} \times X \times 1.240079 \times 10^{-10}$$

where $[C_7H_8]_{in}$ and $[C_7H_8]_{out}$ denoted the inlet and outlet concentrations of toluene, respectively.

3. Results and discussion

3.1. XRD characterization

XRD patterns of samples LMO-SG, LMO-GC and LMO-CP are shown in Fig. 1A. The crystal structure and symmetry of each sample were deduced by referring to the standard powder diffraction file (PDF) in the database of the International Centre of Diffraction Data (ICDD). The characteristic diffraction peaks of sample LMO-SG correlated with those of $LaMnO_{3.26}$ (JCPDS PDF no. 50-0299) structure, which indicated that the perovskite phases corresponding to a rhombohedral symmetry (space group R-3c) was obtained. Differently, sample LMO-GC was typically of a $LaMnO_{3.11}$ (JCPDS PDF no. 50-0297) perovskite structure with an orthorhombic symmetry (space group Pbnm), while XRD patterns of LMO-CP were in good accordance with those of $LaMnO_{3.15}$ (JCPDS PDF no. 50-0298) perovskite, which owned the same symmetry as $LaMnO_{3.26}$. Additionally, no diffraction peaks assignable to the impurities such as La_2O_3 and MnO_x species were observed for samples LMO-SG and LMO-GC, indicating their single perovskite phases. However, as shown in Fig. 1B, a diffraction peak at $2\theta = 28.98°$ was present over sample LMO-CP, which was assigned to the characteristic peak of La_2O_3 (101) phase (JCPDS PDF no. 24-0554). The presence of La_2O_3 impurity was attributed to the surface enrichment of atomic lanthanum without good formation of $LaMnO_3$ perovskite oxide during the calcination process. The crystallite size (d_{XRD}) calculated according to the Scherrer equation ($d_{XRD} = k\lambda/\beta\cos\theta$) and unit-cell parameters of all samples are listed in Table 1. It could be noted that all samples had the similar crystallite size of 14.1(±0.7) nm.

3.2. N_2 sorption

N_2 adsorption–desorption isotherms and pore size distributions of $LaMnO_3$ perovskites oxides prepared by SG, GC and CP methods are presented in Fig. 2A and B, respectively, and their specific surface areas and pore volume are summarized in Table 1. As shown in Fig. 2A, the N_2 adsorption–desorption isotherms of each sample were characteristic of combination of micropore and mesopore structures with a type H3 hysteresis loop in the relative pressure (p/p_0) range of 0.6–1.0. On one hand, there was certain adsorption amount at the initial point of the relative pressure ($p/p_0 = 0$), revealing the existence of micropores in the perovskites. On the other hand, presence of the hysteresis loop indicated the formation of mesopores [18–20], which could be substantiated by the pore-size distributions (Fig. 2B). It was observed that the pore size of each sample was mainly distributed in the range of 10–40 nm. Additionally, for all samples, there was also presence of a small amount of micropores with an intense peak in the range of 1.0–4.0 nm, which agreed well with the isotherms. As seen in Table 1, sample LMO-SG possessed the largest specific surface area and pore volume with values of 35.2 m^2 g^{-1} and 0.243 cm^3 g^{-1}, respectively. Contrarily, sample LMO-GC had the lowest SSA and pore volume values of 21.6 m^2 g^{-1} and 0.072 cm^3 g^{-1}, respectively. It should be noted that the specific surface areas of the prepared samples were much larger than those previously reported in the references [21–23], which could be attributed to great contribution of presence of mesoporous structures in these samples.

3.3. H_2-TPR

In order to investigate the relative reducibility of each sample, H_2-TPR experiments were conducted. H_2-TPR profiles are shown in Fig. 3 and the corresponding H_2 consumption of each reduction region is summarized in Table 2. For all samples, the overall profiles could be divided into three reduction regions, such as the first one in the low temperature range (below 300 °C), the second one

Table 1
Textural properties of all samples.

Samples	Symmetry[a]	d_{XRD}[b] (nm)	Unit-Cell parameters[c]			Vol. (Å^3)	SSA[d] ($m^2\,g^{-1}$)	Pore volume[e] ($cm^3\,g^{-1}$)
			a (Å)	*b* (Å)	*c* (Å)			
LMO-SG	Rhombohedral	13.5	5.4793	5.4793	13.3946	348.3	35.2	0.243
LMO-GC	Orthorhombic	14.7	5.5108	5.4726	7.7526	233.8	21.6	0.072
LMO-CP	Rhombohedral	13.9	5.4968	5.4958	13.3601	349.6	29.4	0.167

[a] Determined from the referenced $LaMnO_{3.26}$ (JCPDS PDF no. 50-0299), $LaMnO_{3.11}$ (JCPDS PDF no. 50-0297) and $LaMnO_{3.15}$ (JCPDS PDF no. 50-0298), respectively.
[b] Calculated from line broadening by the Scherrer equation.
[c] Determined and calculated from XRD patterns by MDI Jade 5.0 program.
[d] Measured from the N_2 adsorption–desorption isotherms by BET method.
[e] Measured from the N_2 adsorption–desorption isotherms by BJH method.

Table 2
The results of quantitative analysis from H_2-TPR profiles.

Samples	H_2-uptakes ($mmol\,g^{-1}$) and temperature of peak maximum (°C)						
	$T^a < 300$	$T_{p.m}$[b]	$300 < T^a < 700$	$T_{p.m.}$	$T^a > 700$	$T_{p.m.}$	Total H_2-uptake
LMO-SG	0.25	259	0.94	441	1.64	863	2.83
LMO-GC	0.06	N.D.	0.69	480	1.73	883	2.48
LMO-CP	0.16	N.D.	1.53	464	1.09	870	2.78

[a] Temperature (°C).
[b] Temperature of peak maximum (°C).

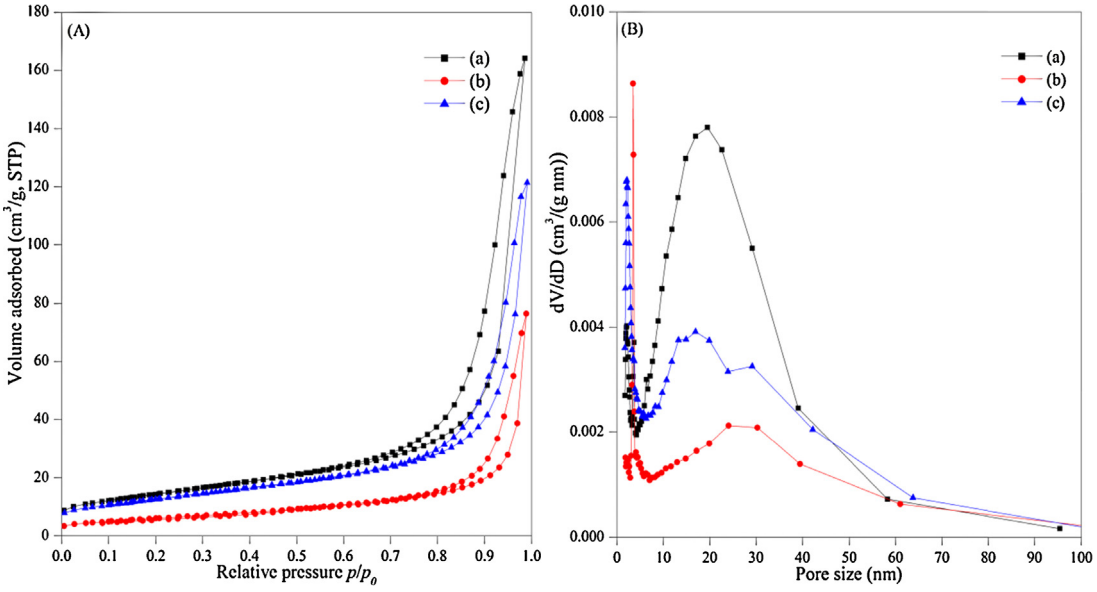

Fig. 2. (A) N_2 adsorption–desorption isotherms and (B) pore-size distributions of samples (a) LMO-SG, (b) LMO-GC and (c) LMO-CP.

in the middle temperature range (300–700 °C) and the third one in the high temperature range (above 700 °C), respectively. In the low temperature region, a relatively small amount of H_2 was consumed below 300 °C with a H_2-uptake of 0.25, 0.06 and 0.16 $mmol\,g^{-1}$ for samples LMO-SG, LMO-GC and LMO-CP, respectively, which could be attributed to removal of some adsorbed oxygen species on the sample surface. Obviously, sample LMO-SG exhibited the largest H_2-consumption with a small shoulder peak at 250 °C, indicating the most outstanding low-temperature reducibility. On the contrary, the signal corresponding to the H_2-consumption of sample LMO-GC was extremely low, suggesting its poor low-temperature reducibility. Larger amounts of H_2 consumption was followed by a broad peak in the temperature range of 300–700 °C and the H_2-uptake was 0.94, 0.69 and 1.53 $mmol\,g^{-1}$ for samples LMO-SG, LMO-GC and LMO-CP, respectively. According to the literatures [24,25], the consumed H_2 in this region participated in the reduction process of Mn^{4+} into Mn^{3+} in perovskite structure. In addition, for sample LMO-SG, the temperatures of peaks maximum in the middle and high temperature regions (441 and 863 °C, respectively) were much lower than those of any other samples, which illustrated that it exhibited an easier reducibility behavior among all samples. Contrarily, sample LMO-GC possessed the worst reducibility owing to its highest temperatures of peaks maximum. In the high temperature region, a greatly intense peak could be observed corresponding to the H_2-uptake of 1.64, 1.73 and 1.09 $mmol\,g^{-1}$ for samples LMO-SG, LMO-GC and LMO-CP, respectively, which correlated with the partial reduction of Mn^{3+} into Mn^{2+}. At even higher temperature, no more H_2-consumption could be observed, which confirmed that a complete reduction of Mn^{2+} cation into metallic manganese would not happen in the reduction process of manganese oxides.

3.4. O_2-TPD

O_2-TPD measurements were performed in order to investigate the surface and bulk oxygen species of the perovskite oxides, and

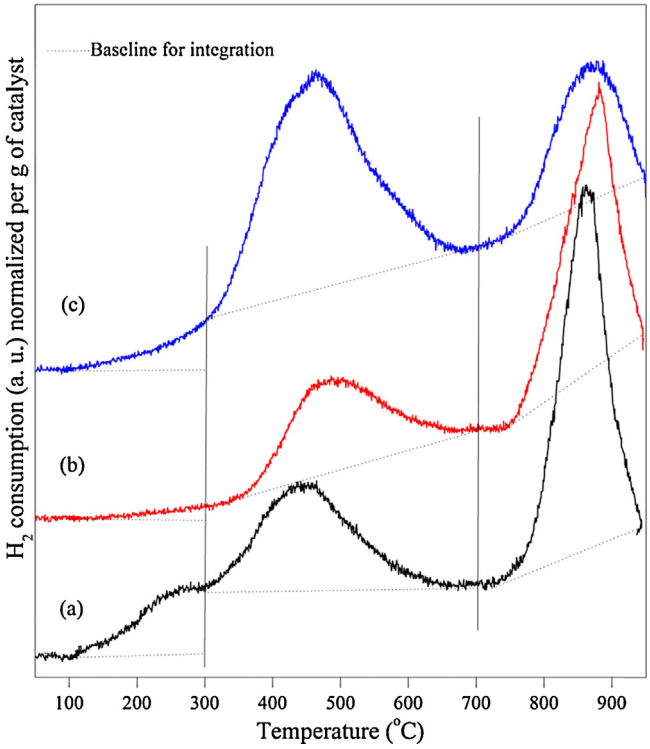

Fig. 3. H_2-TPR profiles of samples (a) LMO-SG, (b) LMO-GC and (c) LMO-CP.

their oxygen desorption profiles within the temperature range of 100–925 °C are depicted in Fig. 4. Apparently, for all samples, three desorption regions could be observed, which were in the temperature range of 100–400 °C, 400–725 °C and 725–925 °C, respectively. The oxygen species desorbed in the first region, denoted as O_α, could be ascribed to the weakest molecular physicsorbed and/or chemisorbed oxygen on the surface [26,27], which can be readily

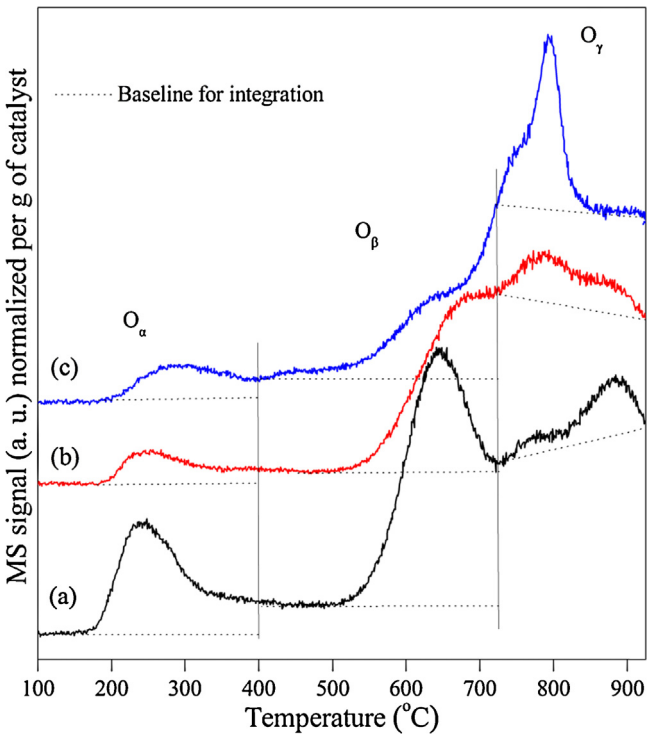

Fig. 4. O_2-TPD profiles of samples (a) LMO-SG, (b) LMO-GC and (c) LMO-CP.

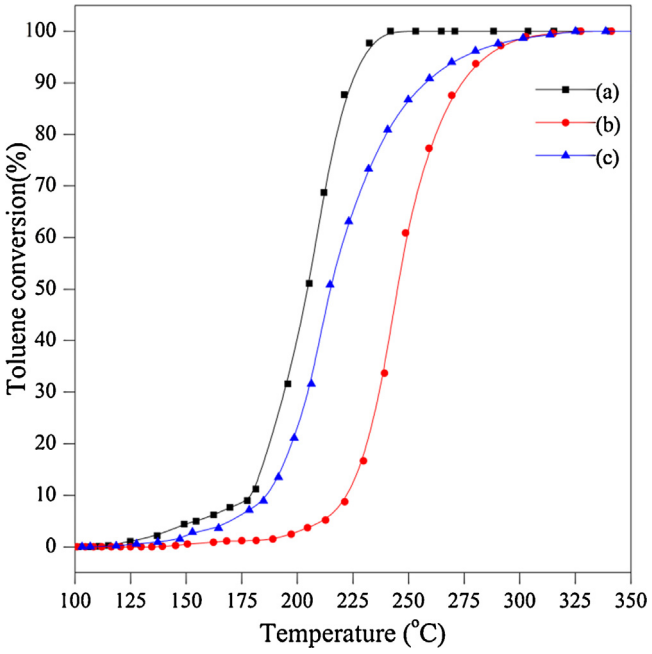

Fig. 5. The light-off curves as a function of reaction temperature for toluene oxidation over samples (a) LMO-SG, (b) LMO-GC and (c) LMO-CP. (The 3rd catalytic run).

removed at relatively low temperature. The oxygen species desorbed in the second region, namely O_β, could be assigned to over-stoichiometric oxygen in the perovskite oxides which may be formulated as the following equation.

$$4Mn^{4+} + 2O^{2-}(\square) \rightarrow 4Mn^{3+} + O_2$$

where the excess oxygen charge was compensated by cation vacancies (□) [28]. The oxygen species desorbed in the higher temperature region, denoted as O_γ, was possibly associated with the migration of lattice oxygen in the bulk perovskite structure. Through quantitative analysis of the profiles, the amount of desorbed oxygen in each region is listed in Table 3. It was observed that the ranking in terms of O_α quantity from the highest to the lowest value was LMO-SG > LMO-CP > LMO-GC, which indicated that $LaMnO_3$ perovskite oxide prepared by citrate sol–gel method exhibited the highest capacity for surface adsorbed oxygen.

3.5. Catalytic performance for toluene oxidation

Measurement of catalytic activity was carried out in the form of light-off experiment, and the catalytic stability of the samples was evaluated under three consecutive light-off runs. Test of catalytic durability was performed in the steady state conditions at 300 °C. Before evaluating the catalytic activity, a blank experiment was performed in the quartz reactor only loaded with quartz wool. The result demonstrated that no homogeneous reactions took place below 350 °C, furthermore, low concentration of toluene was extremely difficult to be oxidized at low temperature directly by thermal incineration.

The catalytic activities of the prepared perovskite oxides for toluene oxidation in the third catalytic run under the reaction conditions are shown in Fig. 5. Apparently, the conversion of toluene monotonously increased with an increase in the reaction temperature, and a complete conversion of toluene could be successfully achieved below 350 °C over all samples. The final products in the reaction were only CO_2 and H_2O, and no other byproducts were detected. Moreover, good carbon balance could be confirmed by the equally similar values of toluene conversion and CO_2

Table 3
The results of quantitative analysis on the O_2-TPD profiles.

Samples	The amounts of desorbed oxygen (mmol g^{-1}) and temperature of peak maximum (°C)						
	O_α (T^a < 400 °C)	$T_{p.m.}$[b]	O_β (400 < T^a < 725 °C)	$T_{p.m.}$	O_γ (T^a > 725 °C)	$T_{p.m.}$	Total desorbed oxygen
LMO-SG	0.0316	241	0.0798	645	0.0143	883	0.1257
LMO-GC	0.0108	250	0.0478	681	0.0150	791	0.0736
LMO-CP	0.0147	280	0.0552	638	0.0216	794	0.0915

[a] Temperature (°C).
[b] Temperature of peak maximum (°C).

Table 4
Temperatures at 10%, 50% and 90% of toluene conversion in three consecutive runs over all samples.

Samples	1st Run			2nd Run			3rd Run		
	T_{10} (°C)	T_{50} (°C)	T_{90} (°C)	T_{10} (°C)	T_{50} (°C)	T_{90} (°C)	T_{10} (°C)	T_{50} (°C)	T_{90} (°C)
LMO-SG	169	193	213	179	203	224	179	204	224
LMO-GC	215	236	260	218	239	266	222	245	274
LMO-CP	180	212	250	182	213	254	184	214	257

selectivity. T_{10}, T_{50} and T_{90}, corresponding to the temperatures at 10, 50 and 90% of toluene conversion, respectively, are used to compare the catalytic activities of the samples and are summarized in Table 4. Among all, sample LMO-SG exhibited the optimum catalytic activity for toluene oxidation with the T_{10}, T_{50} and T_{90} of 179, 204 and 224 °C, respectively, which were 45, 41 and 50 °C lower than those of sample LMO-GC. The ranking in terms of catalytic activity over these perovskite oxides decreased as follows: LMO-SG > LMO-CP > LMO-GC.

In order to test the catalytic stability for toluene oxidation, three consecutive catalytic runs were performed over all samples. The temperatures of T_{10}, T_{50} and T_{90} during the three consecutive runs are summarized in Table 4. Sample LMO-SG exhibited high initial activity in the first catalytic run. In the next two runs, the curves of toluene conversion (not presented here) were nearly overlapped with the similar T_{10}, T_{50} and T_{90} values, which indicated that the catalytic stability was excellent. Even though the occurrence of some degree of deactivation was observed in the second catalytic run with all of T_{10}, T_{50} and T_{90}, 10 °C higher than those observed in the first run, the catalytic performance of LMO-SG in the second and third runs was superior than those of the other two samples in the first run, which verified that LMO-SG was the most efficient catalyst for toluene oxidation. The toluene conversion of sample LMO-CP during the three catalytic runs was similar, which suggested that LMO-CP also exhibited good catalytic stability. However, the overall toluene conversion of sample LMO-GC during the three consecutive catalytic runs gradually shifted towards high temperature, which signified that continuous deactivation occurred on this sample and thus possessed poor catalytic stability for toluene oxidation.

With the object to evaluate the maintenance of long-term activity, a durability test for toluene oxidation over each $LaMnO_3$ perovskite oxide was carried out for 60 h at the reaction temperature of 300 °C, and the curves of toluene conversion versus time on stream are shown in Fig. 6. Obviously, sample LMO-SG exhibited the best catalytic activity and stability, and the conversion of toluene maintained 100% during the period of 60 h, which revealed that under these reaction conditions no deactivation was observed. In spite of a failure to achieve a complete conversion, sample LMO-CP also performed a relatively stable activity with the conversion of toluene above 97% within 60 h under reaction conditions. Moreover, no significant loss of catalytic activity was observed over this sample. However, after a period of 10 h with relatively stable activity, sample LMO-GC became deactivated in the following hours, meanwhile, the conversion of toluene gradually decreased from 100% to 90%, which confirmed its poor durability for toluene oxidation.

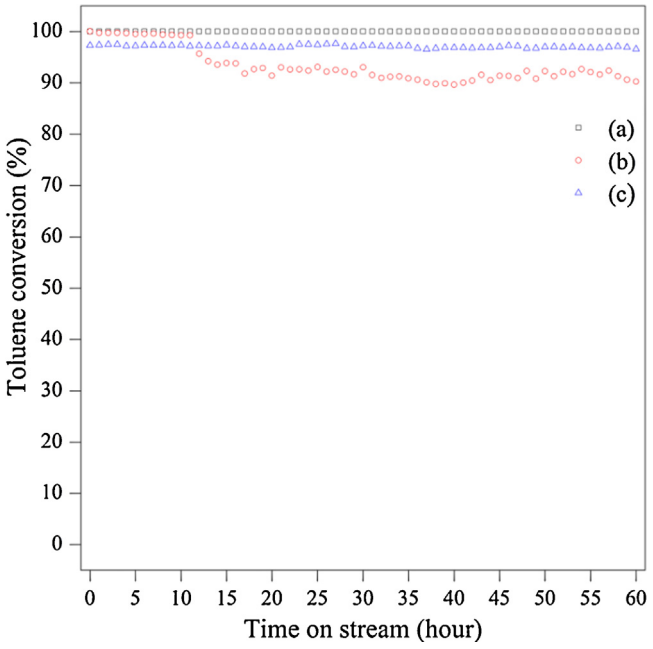

Fig. 6. Toluene oxidation as a function of time on stream over samples (a) LMO-SG, (b) LMO-GC and (c) LMO-CP at 300 °C (reaction conditions: toluene concentration = 1000 ppm, O_2 concentration = 20 vol% and WHSV = 15,000 mL g^{-1} h^{-1}).

Effect of WHSV on the catalytic performance was studied over sample LMO-SG, which was selected as the best-performing catalyst for toluene oxidation. The curves of toluene conversion versus reaction temperature at different WHSV are shown in Fig. 7. As expected, the catalytic activity decreased with an increase in WHSV values. When WHSV was 10,000 mL g^{-1} h^{-1}, the corresponding T_{10}, T_{50} and T_{90} values were 159, 183 and 204 °C, respectively, which were 10, 10 and 9 °C lower than those achieved at WHSV of 15,000 mL g^{-1} h^{-1}. The further increase in WHSV from 15,000 to 30,000 and continuously to 60,000 mL g^{-1} h^{-1} resulted in an obvious drop in catalytic activity. Whatever WHSV studied, complete oxidation of toluene was observed above 300 °C.

It has been reported that specific surface area, low-temperature reducibility and available oxygen species on the catalyst surface are key factors to influence the oxidation activity of perovskite catalysts [29,30]. The higher specific surface area implies more available active sites on the catalysts, which is beneficial for the enhancement of catalytic activity. Moreover, a porous structure

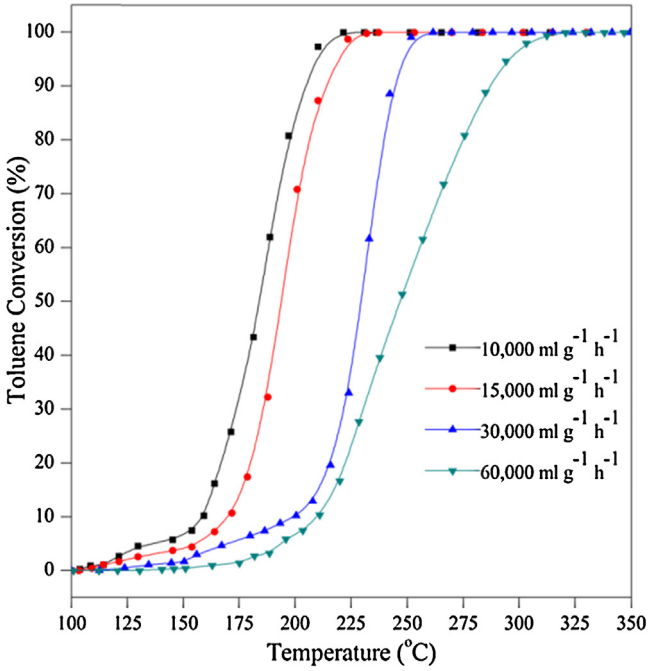

Fig. 7. Effect of WHSV on toluene oxidation over sample LMO-GC (reaction conditions: toluene concentration = 1000 ppm and O_2 concentration = 20 vol%).

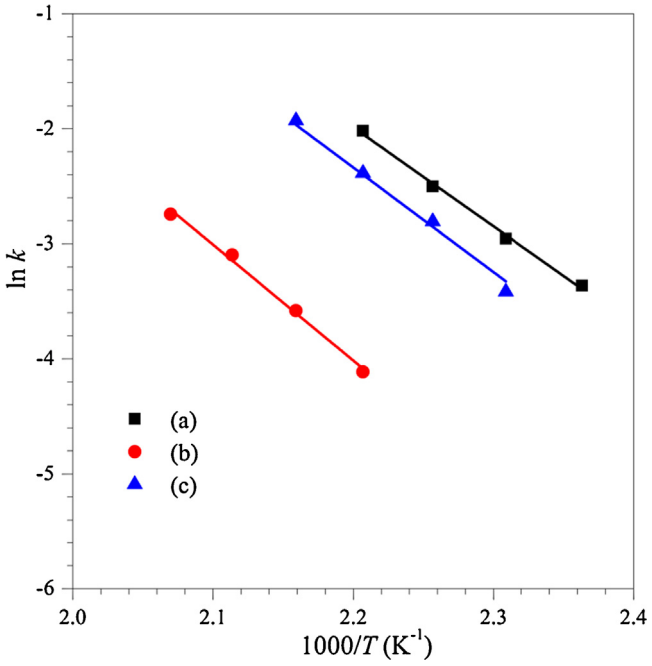

Fig. 8. Arrhenius plots for toluene oxidation over samples (a) LMO-SG, (b) LMO-GC and (c) LMO-CP (reaction conditions: toluene concentration = 1000 ppm, O_2 concentration = 20 vol% and WHSV = 15,000 mL g^{-1} h^{-1}).

with high pore volume is also favorable to facilitate the adsorption and diffusion of reactant molecules, thus promoting the catalytic performance. The reducibility of perovskite catalysts closely correlates with the redox ability of B-site cations (Mn^{4+}/Mn^{3+} and Mn^{3+}/Mn^{2+} redox couples in this study). From this viewpoint, low-temperature reducibility surely has a significant effect on the catalytic performance for oxidation reactions at relatively low temperature (below 400 °C). Surface adsorbed oxygen, the most active species, has been proven to play an important role in the catalytic oxidation of numerous VOCs [11,12,29]. Especially for the toluene oxidation over perovskite oxides, which was reported to obey a suprafacial catalytic mechanism proposed by Voorhoeve et al. [31], more available adsorbed oxygen on the catalyst surface could promote the interaction with reactants at low temperature, thus enhancing the catalytic performance.

In order to investigate the internal relationship between these parameters and the catalytic performance, a comprehensive analysis was made based on the results of catalyst characterizations and catalytic activity tests. It was clearly found that sample LMO-SG with higher specific area and stronger low-temperature reducibility exhibited better catalytic performance for toluene oxidation in comparison with the other two samples. In addition, larger amounts of adsorbed oxygen species were present on the surface of sample LMO-SG according to O_2-TPD result, which was another reason responsible for its superior catalytic performance. Therefore, it can be concluded that the excellent catalytic performance of LMO-SG might be associated with its higher specific surface area, better low-temperature reducibility and more surface oxygen species. To consider the results of catalytic activity, stability and durability tests, the ranking in terms of catalytic performances over these catalysts from the best to the worst was as following LMO-SG > LMO-CP > LMO-GC, which was in good agreement with the results obtained from BET, H_2-TPR and O_2-TPD characterizations. This observation could confirm the correlation between the catalytic performances and the physicochemical properties of these perovskite oxides.

3.6. Calculation of apparent activation energy

During the past periods, many researchers focused their attentions on the kinetics study for the catalytic oxidation of VOCs [32–34]. For example, Baylet et al. [33] carried out the parametric study of propene oxidation over supported Pt and Au catalysts, which found that the propene oxidation rate was only dependent on the oxygen partial pressure over all Pt catalysts. Gutiérrez-Ortiz et al. [34] did kinetical analysis of 1,2-dichloroethane (DCE) oxidation over nanocrystalline Co_3O_4 catalysts, considering pseudo-first order kinetics in DCE, zero order for oxygen (due to its excess concentration) and an Arrhenius dependence of the rate constant. To assume a first-order kinetics with respect to toluene and a zero-order to oxygen, Dai et al. obtained good linear Arrhenius plots for the oxidation of toluene over $LaMnO_3$, $Eu_{1-x}Sr_xFeO_3$ and $La_{0.6}Sr_{0.4}CoO_3$ supported Co_3O_4 catalysts [30,19,35]. Hence, in this work, it is also reasonably assumed that in the presence of excess oxygen (volumetric concentration = 20%), the reaction would obey a first-order kinetical mechanism towards toluene concentration i.e., $r = kc = (A\exp(-E_a/RT))c$, where r, k, c, A, and E_a are the reaction rate (mol g^{-1} s^{-1}), rate constant (s^{-1}), toluene concentration (mol g^{-1}), pre-exponential factor (s^{-1}) and apparent activation energy (kJ mol^{-1}), respectively. The Arrhenius plots for toluene oxidation over all perovskite oxides are shown in Fig. 8, and the kinetic parameters calculated from the data of catalytic activity at the toluene conversion less than 20%, in order to be in chemical regime, are summarized in Table 5. It can be clearly observed that the Arrhenius plots of all samples were in good linear relationship. Moreover, the E_a values for toluene oxidation over these samples decreased in the ranking LMO-GC > LMO-CP > LMO-SG, where the lowest E_a value (71 kJ mol^{-1}) was obtained over sample LMO-SG. These results indicated that the oxidation of toluene could proceed more readily over sample LMO-SG, which was good consistence with its optimum catalytic performance. The E_a values and some other representative results for toluene oxidation over the perovskite and transition metal oxides, which have been previously reported in the literatures [29,34,36–39],

Table 5
Rate constants (k), reaction rates (r), pre-exponential factors (A) and activation energies (E_a) for oxidation of toluene over all samples (reaction conditions: toluene concentration = 1000 ppm, O_2 concentration = 20 vol% and WHSV = 15,000 mL g^{-1} h^{-1}) and contrastive results previously reported in literatures.

Samples	k ($\times 10^{-2}$ s^{-1})/r ($\times 10^{-9}$ mol g^{-1} s^{-1})							A ($\times 10^7$ s^{-1})	E_a (kJ mol^{-1})	R^2
	150 °C	160 °C	170 °C	180 °C	190 °C	200 °C	210 °C			
LMO-SG	3.47/6.23	5.21/9.21	8.20/14.10	13.30/21.84	–	–	–	2.23	71	0.9966
LMO-GC	–	–	–	1.64/2.99	2.78/5.04	4.53/8.05	6.44/11.25	7.63	84	0.9950
LMO-CP	–	–	6.04/10.60	9.19/15.66	14.52/23.59	–	–	4.69	76	0.9902
Compared samples	Calcination conditions	SSA (m^2 g^{-1})	Temperature (°C)	Toluene conversion (%)	Cited reference					
LMO-SG	750 °C (2 h) in air	35.2	204	50	This work	2.23	71	–		
LMO-GC	750 °C (2 h) in air	21.6	245	50	This work	7.63	84			
LMO-CP	750 °C (2 h) in air	29.4	214	50	This work	4.69	76			
Bulk $LaMnO_3$	850 °C (4 h) in air	7.3	267	50	[29]	425	97			
3DOM[a] $LaMnO_3$	750 °C (4 h) in air	37.7	232	50	[29]	0.14	62			
Bulk $EuFeO_3$	750 °C (4 h) in air	2.9	360	50	[34]	31.5	104			
3DOM $Eu_{0.6}Sr_{0.4}FeO_3$	750 °C (4 h) in air	31.3	278	50	[34]	3.57	81			
$La_{0.6}Sr_{0.4}Fe_{0.8}Bi_{0.2}O_3$	750 °C (4 h) in air	21.6	256	50	[35]	0.13	74			
Bulk $LaFeO_3$	700 °C in air	21.0	323	50	[36]	n.e.[b]	153			
Bulk $LaNiO_3$	700 °C in air	14.0	297	50	[36]	n.e.	100			
CuO/Al_2O_3	450 °C (2 h) in air	151.0	n.e.	50	[37]	n.e.	94			
MnO_x/Al_2O_3	450 °C (2 h) in air	122.0	n.e.	50	[37]	n.e.	126			
$Ni_{0.5}Zn_{0.5}Fe_2O_4$	850 °C (3 h) in air	2.8	n.e.	50	[38]	n.e.	124			

[a] 3DOM: Three dimensional ordered macroporous.
[b] n.e.: not estimated.

are also summarized in Table 5. Through a comparative analysis, it can be clearly observed that the apparent activation energies for toluene oxidation obtained over our prepared $LaMnO_3$ perovskite oxides, which were in the range of 71–84 kJ mol^{-1}, were greatly close to those of 3DOM $Eu_{0.6}Sr_{0.4}FeO_3$ (81 kJ mol^{-1}) and $La_{0.6}Sr_{0.4}Fe_{0.8}Bi_{0.2}O_3$ (74 kJ mol^{-1}) perovskites, and much lower than those of bulk $LaMnO_3$, $EuFeO_3$, $LaFeO_3$ and $LaNiO_3$ perovskite oxides (97–153 kJ mol^{-1}) as well as $Ni_{0.5}Zn_{0.5}Fe_2O_4$ and Al_2O_3 supported CuO or MnO_x (94–126 kJ mol^{-1}). However, the synthesized 3DOM $LaMnO_3$ perovskite oxide via a templating-generation in [29] presented a lower E_a value in comparison with our $LaMnO_3$ catalysts via a conventional sol–gel route, which indicated the significant role of preparation method in morphology control and catalytic activity modification. Moreover, the pre-exponential factor of A is considered to be related with the conversion rate of the activated reactant molecules into products in the molecular collision theory. Normally, the lower the pre-exponential factor is, the higher the conversion rate is. It was observed that the pre-exponential factors obtained over our $LaMnO_3$ catalysts were much higher than that of 3DOM $LaMnO_3$ perovskite oxide. These comparative results inferred that $LaMnO_3$ catalysts with special morphologies and structures would accelerate the conversion rate of toluene, consequently exhibiting higher catalytic activities than those of ordinary bulk $LaMnO_3$ perovskite oxides.

4. Conclusions

$LaMnO_3$ perovskite oxides were synthesized by citrate sol–gel (SG), glycine combustion (GC) and co-precipitation (CP) methods, respectively. Their catalytic performances were evaluated for catalytic oxidation of toluene. Results showed that a complete conversion of toluene could be achieved over all perovskite oxides below 350 °C in three consecutive catalytic runs. Among all, sample LMO-SG exhibited superior catalytic activity, stability and durability for toluene oxidation, which was greatly attributed to its higher specific surface area, better low-temperature reducibility and more surface adsorbed oxygen species. Furthermore, good linear Arrhenius plots were obtained over all perovskite oxides, and the apparent activation energy of LMO-SG for toluene oxidation was lower than those of LMO-GC and LMO-CP, confirming its optimum catalytic performance. Finally, thanks to comparison with literature data, the morphology and the structure are also key parameters to achieve high catalytic oxidation performance.

Acknowledgments

This work was financially supported by National Basic Research Program of China (2010CB732300, 2013CB933201), National High Technology Research and Development Program of China (2011AA03A406) and 111 Project (B08021), Université Lyon 1 and CNRS. The authors gratefully acknowledge China Scholarship Council for the Joint-Training Scholarship Program with Institut de Recherches sur la Catalyse et l'Environnement de Lyon (IRCELYON) and Université Claude Bernard Lyon 1(UCBL1).

References

[1] H.L. Chen, H.M. Lee, S.H. Chen, M.B. Chang, S.J. Yu, A.S. Nan Li, Environmental Science &Technology 43 (2009) 2216–2227.
[2] W.B. Li, J.X. Wang, H. Gong, Catalysis Today 148 (2009) 81–87.
[3] J. Fenger, Atmospheric Environment 43 (2009) 13–22.
[4] Thematic Strategy on Air Pollution, Communication from the Commission to the Council and The European Parliament, Commission of the European Communities, COM (2005) 446 final, Brussels, 2005.
[5] Contents of new emission regulation of volatile organic compounds, Press release2005, Ministry of Environment, Government of Japan.
[6] M. Paulis, L.M. Gandı´a, A. Gil, J. Sambeth, J.A. Odriozola, M. Montes, Applied Catalysis B: Environmental 26 (2000) 37–46.

[7] S. Ordóñez, L. Bello, H. Sastre, R. Rosal, F.V. Díez, Applied Catalysis B: Environmental 38 (2002) 139–149.
[8] W.B. Li, W.B. Chu, M. Zhuang, J. Hua, Catalysis Today 93–95 (2004) 205–209.
[9] Q. Yan, X. Li, Q. Zhao, G. Chen, Journal of Hazardous Materials 209–210 (2012) 385–391.
[10] B.P. Barbero, L. Costa-Almeida, O. Sanz, M.R. Morales, L.E. Cadus, M. Montes, Chemical Engineering Journal 139 (2008) 430–435.
[11] N.A. Merino, B.P. Barbero, P. Grange, L.E. Cadús, Journal of Catalysis 231 (2005) 232–244.
[12] C. Zhang, C. Wang, W. Zhan, Y. Guo, Y. Guo, G. Lu, A. Baylet, A. Giroir-Fendler, Applied Catalysis B: Environmental 129 (2013) 509–516.
[13] G. Pecchi, P. Reyes, R. Zamora, L.E. Cadús, J.L.G. Fierro, Journal of Solid State Chemistry 181 (2008) 905–912.
[14] R. Spinicci, M. Faticanti, P. Marini, S. De Rossi, P. Porta, Journal of Molecular Catalysis A: Chemical 197 (2003) 147–155.
[15] M.C. Álvarez-Galván, V.A. de la Peña O'Shea, G. Arzamendi, B. Pawelec, L.M. Gandía, J.L.G. Fierro, Applied Catalysis B: Environmental 92 (2009) 445–453.
[16] S. Brunauer, P.H. Emmett, E. Teller, Journal of the American Chemical Society 60 (1938) 309–319.
[17] E.P. Barrett, L.G. Joyner, P.P. Halenda, Journal of the American Chemical Society 73 (1951) 373–380.
[18] X. Wang, X. Zhang, Y. Wang, H. Liu, J. Qiu, J. Wang, W. Han, K.L. Yeung, Chemistry of Materials 23 (2011) 4469–4479.
[19] K. Ji, H. Dai, J. Deng, H. Jiang, L. Zhang, H. Zhang, Y. Cao, Chemical Engineering Journal 214 (2013) 262–271.
[20] B. Pawelec, V. La Parola, R.M. Navarro, S. Murcia-Mascarós, J.L.G. Fierro, Carbon 44 (2006) 84–98.
[21] H.J. Wei, Y. Cao, W.J. Ji, C.T. Au, Catalysis Communications 9 (2008) 2509–2514.
[22] R. Hammami, S.B. Aïssa, H. Batis, Applied Catalysis A: General 353 (2009) 145–153.
[23] Z. Wei, L. Wei, L. Gong, Y. Wang, C. Hu, Journal of Hazardous Materials 177 (2010) 554–559.
[24] S. Irusta, M.P. Pina, M. Menéndez, J. Santamarıa, Journal of Catalysis 179 (1998) 400–412.
[25] A. Kaddouri, S. Ifra, Catalysis Communication 7 (2006) 109–113.
[26] S. Liang, T. Xu, F. Teng, R. Zong, Y. Zhu, Applied Catalysis B: Environmental 96 (2010) 267–275.
[27] H.M. Zhang, Y. Shimizu, Y. Teraoka, N. Miura, N. Yamazoe, Journal of Catalysis 121 (1990) 432–440.
[28] J.A.M. van Roosmalen, E.H.P. Cordfunke, R.B. Helmholdt, H.W. Zandbergen, Journal of Solid State Chemistry 110 (1994) 100–105.
[29] C. Zhang, W. Hua, C. Wang, Y. Guo, Y. Guo, G. Lu, A. Baylet, A. Giroir-Fendler, Applied Catalysis B: Environmental 134–135 (2013) 310–315.
[30] Y. Liu, H. Dai, Y. Du, J. Deng, L. Zhang, Z. Zhao, C.T. Au, Journal of Catalysis 287 (2012) 149–160.
[31] R.J. Voorhoeve, J.P. Remeika, D.W. Johnson Jr., Science 180 (1973) 62–64.
[32] S. Benard, A. Baylet, P. Vernoux, J.L. Valverde, A. Giroir-Fendler, Catalysis Communications 36 (2013) 63–66.
[33] A. Baylet, C. Capdeillayre, L. Retailleau, J.L. Valverde, P. Vernoux, A. Giroir-Fendler, Applied Catalysis B: Environmental 102 (2011) 180–189.
[34] B. de Rivas, R. López-Fonseca, C. Jiménez-González, J.I. Gutiérrez-Ortiz, Chemical Engineering Journal 184 (2012) 184–192.
[35] X. Li, H. Dai, J. Deng, Y. Liu, Z. Zhao, Y. Wang, H. Yang, C.T. Au, Applied Catalysis A: General 458 (2013) 11–20.
[36] Z. Zhao, H. Dai, J. Deng, Y. Du, Y. Liu, L. Zhang, Journal of Molecular Catalysis A: Chemical 366 (2013) 116–125.
[37] G. Pecchi, M.G. Jiliberto, E.J. Delgado, L.E. Cadús, J.L.G. Fierro, Journal of Chemical Technology and Biotechnology 86 (2011) 1067–1073.
[38] S.M. Saqer, D.I. Kondarides, X.E. Verykios, Applied Catalysis B: Environmental 103 (2011) 275–286.
[39] M. Florea, M. Alifanti, V.I. Parvulescu, D. Mihaila-Tarabasanu, L. Diamandescu, M. Feder, C. Negrila, L. Frunza, Catalysis Today 141 (2009) 361–366.